

Learning to Navigate using Visual Sensor Networks

Jan Blumenkamp¹ Qingbiao Li¹ Binyu Wang Zhe Liu¹ Amanda Prorok¹

¹Department of Computer Science and Technology
University of Cambridge

Abstract: We consider the problem of navigating a mobile robot towards a target in an unknown environment that is endowed with visual sensors, where neither the robot nor the sensors have access to global positioning information and only use first-person-view images. While prior work in sensor network based navigation uses explicit mapping and planning techniques, and are often aided by external positioning systems, we propose a vision-only based learning approach that leverages a Graph Neural Network (GNN) to encode and communicate relevant viewpoint information to the mobile robot. During navigation, the robot is guided by a model that we train through imitation learning to approximate optimal motion primitives, thereby predicting the effective cost-to-go (to the target). In our experiments, we first demonstrate generalizability to previously unseen environments with various sensor layouts. Our results show that by using communication between the sensors and the robot, we achieve up to $2.0\times$ improvement in SPL (Success weighted by Path Length) when compared to the communication-free baseline. This is done without requiring a global map, positioning data, nor pre-calibration of the sensor network. Second, we perform a zero-shot transfer of our model from simulation to the real world. To this end, we train a ‘translator’ model that translates between latent encodings of real and simulated images so that the navigation policy (which is trained entirely in simulation) can be used directly on the real robot, without additional fine-tuning. Physical experiments demonstrate the feasibility of our approach in various cluttered environments.

Keywords: Visual Navigation, Mobile Robots, Sensor Networks, Graph Neural Networks, Imitation Learning

1 Introduction

Efficiently finding and navigating to a target in complex unknown environments is a fundamental robotics problem, with applications to search and rescue [1], surveillance [2], and monitoring [3]. This paper focuses on navigating an unknown environment to find a target under the guidance of a static *visual sensor network*. Prior work has provided effective solutions employing low-cost wireless sensors to guide robotic navigation [3, 4]. These studies demonstrate that at a small additional cost—i.e., the deployment of cheap static sensors with local communication capabilities—the requirements on the robot’s capabilities can be significantly reduced while simultaneously improving its navigation efficiency.

However, the implementation of traditional sensor network guided navigation is cumbersome. It commonly consists of five main steps: (1) estimate robot and sensor positions through external positioning systems, (2) process sensor data to detect the target, (3) transmit target information to the robot, (4) build the environmental map and plan a target path, and (5) control the robot to follow the path according to its motion model. This framework has several drawbacks. First, parameters need to be hand-tuned, and data pre-processing steps are required. Second, isolating the perception, planning, and control modules hinder potential positive feedback among them, and make the modeling and control problems challenging. Finally, this approach requires the availability of an absolute positioning system, to build on step (1).

In this paper, we consider a learning-based approach by introducing a static visual sensor network that is capable of learning to guide a robot to the target. The nodes in this sensor network are endowed with policies that are learned through a machine learning architecture that leverages a Graph Neural Network (GNN). Successful navigation requires the robot to learn the relationship between its surrounding environment, raw sensor data, and its actions. Our contributions are as following:

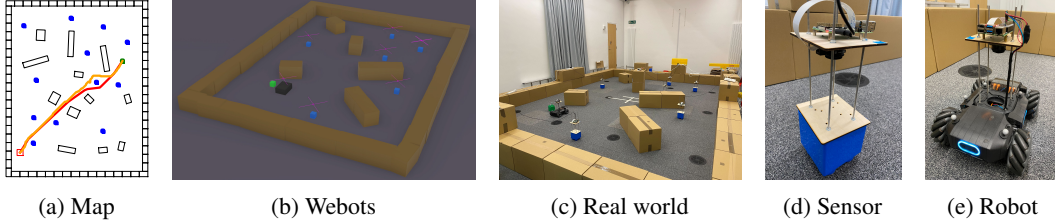


Figure 1: Our setup consists of (a) an environment populated with obstacles, visual sensors (blue), a mobile robot equipped with a sensor, and a green target, where the mobile robot has to find the shortest path (red, taken path orange) to an occluded target by incorporating communicated sensor information to enhance its navigation performance. Our framework leverages a setup consisting of a simulation environment (b) that corresponds to the real-world setup (c). The workspace is endowed with custom-built sensors with fish-eye cameras (d, e) that are capable of communicating with each other. One sensor is attached to a mobile robot (e) that acts on the output of that sensor.

- We present a framework that demonstrates, for the first time, how low-cost sensor networks can help robots navigate to targets in unknown environments, where neither the robot nor the sensors possess any absolute positioning information.
- We provide an end-to-end visual navigation policy that leverages the expressive power of GNNs to learn what needs to be communicated and how to aggregate the visual scene for effective navigation.
- Experimental results demonstrate generalizability to unseen environments with various sensor layouts. In particular, by introducing a real-to-sim image translator, our policy (which is trained entirely in simulation) can be transferred to the real world without additional tuning (i.e., in a zero-shot manner).

2 Related Work

Sensor Network-Guided Navigation. Most of early approaches for sensor network-guided robot navigation assume that either the robot [3, 5] or the sensors [6, 7] are fully positioned in an absolute reference frame, so that an explicit environment map can be created. This information is leveraged to plan the shortest multi-hop route from sensor to sensor, eventually arriving at the target. Shah et al [8] propose a vision-based decentralized controller to aggregate a swarm of agents without relying on inter-agent communication. Methods such as Gaussian Belief Propagation [9] or Factor Graphs [10] use probabilistic models to estimate information such as the position of nodes in a graph using local information iteratively in a computationally efficient manner, which are typically used in robot mapping. These methods require human prior knowledge to design and tune the model and to extract relevant local features. In contrast, our method is completely data-driven and trained end-to-end, using visual images to directly navigate the robot towards its destination in an unknown environment. Our method promises to scale to any complex real-world scene, where feature extraction for the use of previously mentioned methods can be challenging. Deep Learning (DL)-based methods are becoming more attractive, but approaches such as [11], still require anchor-nodes with access to global positioning information. To the best of our knowledge, there is no related work that uses first-person-view visual observations.

Visual navigation. Learning efficient features from the raw image data is challenging. Hence, auxiliary tasks [1, 12] are used to increase the quality of extracted feature. Curriculum learning [12] is often used for overcoming low sample efficiency and reward sparsity. In contrast to prior work, we consider a novel problem formulation in which the navigating robot is guided by a network of visual sensor that are communicating with the robot and amongst each other. Instead of introducing auxiliary tasks or learning curricula, we use a joint training scheme to directly learn what information needs to be communicated and how to aggregate the communicated information to ensure efficient navigation in unknown environments.

GNNs for sensor networks and mobile robot systems. As an effective method to aggregate and learn from relational, non-Euclidean data, GNNs have achieved promising results in numerous domains [13]. In [14, 15], a fully decentralized local motion coordination framework is proposed to solve the multi-robot path-planning problem. In [16], GNNs are used to elicit adversarial communications for self-interested objectives. However, these methods have not considered first-person-view observations. VGAI [17] uses first-person view visual information to imitate a flocking policy in a swarm of drones using GNNs. That

problem is different, though, since it is sufficient to extract proximity information from the local robot neighborhood for a reasonable flocking policy. On the other hand, for target navigation, information about the direction to the target has to propagate through the network and reach the navigating robot such that it moves along the shortest collision-free path. Furthermore, no real-world experiments were conducted.

Imitation Learning for Navigation. In its early phases, IL was addressed as a standard supervised learning problem. This approach assumes that data are i.i.d, which is not true as a learned policy influences the future test inputs on which it will be evaluated. This can be alleviated by training over multiple rounds of interaction [18]. DAGGER is able to learn a stationary deterministic policy guaranteed to perform well under its induced distribution of states improves by using reduction-based approaches that enable using supervised learning [19]. AGGREGATE improves further on this by iteratively estimating a cost-to-go function [20]. Traditional approaches for navigation in unknown environments usually utilize the greedy search with Euclidean heuristic or Manhattan heuristic, which are in-efficient in detecting and escaping local minima [21]. Recent learning-based approaches imitate oracles such as MPC to offer better sample efficiency [22]. In this paper, we employ a visual sensor network to implicitly learn the cost-to-go by predicting the direction corresponding to the shortest path to the target.

Sim-to-Real Transfer and Real-World GNN Implementation. The gap between the simulator and the real world, where dynamics and vision differ, makes it difficult to transfer learned policy. RCANs [23] are proposed to close the gap without using real-world data. Church et al. [24] use image-to-image translation [25] to minimize the difference between real and simulated tactile images. VR-Goggles [26] uses a real-to-sim approach to sim-to-real transfer, where real-world images are first transformed into simulated images, based on a modified CycleGAN [27], so that the policy trained in simulation can be directly deployed. In this paper, we leverage GNNs for robot navigation tasks. Recent work [28] builds the first real-world deployment of GNN-based policies on a decentralized multi-robot platform, but relies on global positioning and a relatively simple state space.

3 Problem Formulation

Our setup consists of a cluttered environment, a mobile robot, and a set of visual sensors. The environment \mathcal{W} contains a set of randomly placed static obstacles $\mathcal{C} \subset \mathcal{W}$ and N randomly placed visual sensors $S = \{S^1, \dots, S^N\}$. As shown in Fig. 1 (c), at every time step t , each sensor S^i is capable of taking an omnidirectional RGB image o_t^i of its surrounding environment, but has *no positioning information*. Each sensor S^i can communicate with nearby sensors within communication range, i.e., $S^j \in \mathcal{N}^i$. A target object G is located randomly in the 2D ground plane at position q^G . Each sensor predicts the direction $u_t^i \in \mathcal{U}$ along the shortest path towards the target G . The mobile robot R is located at position q_t^R and moves in the ground plane in $\mathcal{W} \setminus \mathcal{C}$. It is equipped with *any one* of the sensors (we choose sensor S^1) and uses the directional output u_t^1 of that sensor to execute an action $a_t \in \mathcal{A}$ by applying a velocity of the same direction. *The robot’s objective is to move to the target G along the shortest collision-free path. It utilizes the information shared through the sensor network to make an informed decision about how to reach the (potentially occluded) target, while avoiding time-consuming exploration.*

We formalize this as a sequential decision making problem under uncertainty about the underlying world [29], and define a corresponding Markov Decision Process (MDP). At time step t , let $s_t \in \mathcal{O}$ be the observed state of the environment, i.e $s_t = \{o_t^1, \dots, o_t^N\}$. On executing a_t , the new state s_{t+1} is determined by the underlying world \mathcal{W} , which is a hidden variable, sampled from a prior $P(\mathcal{W})$ and in turn induces a state transition distribution $P(s_{t+1}|s_t, a_t)$. The one-step cost $c(s_t, a_t)$ is the distance travelled since the previous time step and a consequence of action a_t .

Let $\pi(s_t)$ be a policy that maps the state s_t to an action a_t . The policy represents the navigation strategy that we wish to learn. An episode continues until either the goal is reached ($\|q^G - q_t^R\| < D_G$) or time horizon T is reached. Given a prior distribution over worlds $P(\mathcal{W})$ and a distribution over start and goal positions $P(q_0^R, q^G)$, we can estimate the cost of moving from position q_0^R to q^G as

$$V(s_t) = \sum_{t=1}^T \mathbb{E}_{s_t \sim d_\pi^t} [c(s_t, \pi(s_t))] \quad (1)$$

where $d_\pi^t = P(s_t|\pi, \mathcal{W}, q_t, q^G)$ is the distribution over states induced by running π on the problem (\mathcal{W}, q_t, q^G) for T steps [30], and we evaluate the performance of a policy as

$$J(\pi) = \mathbb{E}_{\substack{\mathcal{W} \sim P(\mathcal{W}), \\ (q_0^R, q^G) \sim P(q_0^R, q^G)}} [V(s_t)]. \quad (2)$$

Assumptions. The robot has no knowledge of its own position, nor the environment map, nor the target location. The target has to be within visibility range at least one sensor within multi-hop communication to the robot, but it is not necessary for the robot itself to observe the target. In order for the sensors to be able to localize themselves within the environment and with respect to the robot, a minimum overlapping field of view is required. We do not assume any ordering or identification of sensor nodes. Our approach is stateless, and we do not use memory to store information over multiple time steps (i.e., we do not build a map).

4 Visual Navigation using Sensor Networks

This section describes our approach to training the navigation policy π . Fig. 1 shows the simulation environment and Fig. 2 shows an overview of our architecture. The objective of each sensor S^i is to predict a direction u_t^i along the shortest path to the target (with the consideration of static obstacles) by using its own observation o_t^i and the messages shared by other sensors. We use a variant of Imitation Learning (IL) using expert solvers (i.e., cheap and fast path planning algorithms).

Our method does not rely on any positioning information whatsoever, and as explained in Sec. 3, the neighborhood \mathcal{N}^i is defined through sensors within communication range. During training and evaluation in simulation, we have to model this communication range. We assume a disk model, where the neighbor set is defined as $\mathcal{N}^i = \{S^j | L(S^i, S^j) \leq D_S\}$, where $L(S^i, S^j)$ is the euclidean distance between S^i and S^j , and D_S is the communication range.

In Sec. 4.1, we explain how we generate the dataset $\mathcal{D}_{\text{IL}} = \{(o_0^{i,m}, \hat{A}_0^{i,m})\}_{m=1, i=1}^{M,N}$ consisting of M per-sensor cost-to-go advantage labels \hat{A} and observations o . In Sec. 4.2, we detail the neural network model $\psi \circ \theta \circ \phi(\cdot)$ consisting of the feature extractor ϕ , the feature aggregator θ and the post-processor ψ to predict the advantages. The architecture is depicted in Fig. 2. This neural network is optimized with the objective J_{IL} as

$$J_{\text{IL}}(\psi \circ \theta \circ \phi) = \mathbb{E}_{o, \hat{A} \sim \mathcal{D}_{\text{IL}}} \left[\|\psi \circ \theta \circ \phi(o) - \hat{A}\|^2 \right]. \quad (3)$$

While we train our policy in simulation, we take an approach that facilitates sim-to-real transfer (see Sec. 5).

4.1 Data Generation

Imitation learning can be treated as supervised learning problem. Since future states are influenced by previous actions in IL, the i.i.d. assumption of supervised learning is invalidated. AGGREGATE [20] proposes one possible solution to this problem by iteratively learning cost-to-go estimates for trajectories of data using an online procedure. For the type of navigation policy that we wish to learn, it is trivial to compute cost-to-go estimates, and therefore we treat it as standard supervised learning problem with an i.i.d. assumption for each sample.

Let Q^i be the cost-to-goal for sensor S^i . Let the set of possible directions be $\mathcal{U} = \{u^1, \dots, u^K\}$. Let $Q_{u^k}^i$ be the cost-to-goal for sensor S^i upon moving towards direction u_k^i . To simplify the training procedure and facilitate better generalization, instead of learning absolute cost-to-goal values Q^i , we learn a relative cost-advantage vector $A^i = [Q_{a1}^i - Q^i, \dots, Q_{ak}^i - Q^i]^\top$ that subtracts the cost from the current state to the goal for each of the K possible directions and thus is scale-invariant (since the scale of the cost-to-go values are not relevant for a sequential decision making problem).

We generate the dataset \mathcal{D}_{IL} consisting of $M = 40,000$ environment samples for $N = 7$ sensors for training the policy π . We provide further details on the dataset and the training in Appendix A.

4.2 GNN-based Feature Aggregation across Sensor Network

The neural network is homogeneous across all sensors (and robot) and is divided into the three sub-modules feature extractor $\phi(\cdot)$, feature aggregator $\theta(\cdot)$ and post-processor $\psi(\cdot)$.

Local feature extraction. We first use a Convolutional Neural Network (CNN) $\phi(\cdot)$, specifically MobileNet v2 [31], to extract features z_t^i from the image o_t^i of each sensor S^i . MobileNet is optimized for the evaluation on mobile devices, which makes it an ideal candidate for the application in a distributed sensor network. For the sim-to-real transfer, we replace the encoder, as explained in detail in Sec. 5 and visualized in Fig. 2. The encoding is communicated to other sensors within communication range.

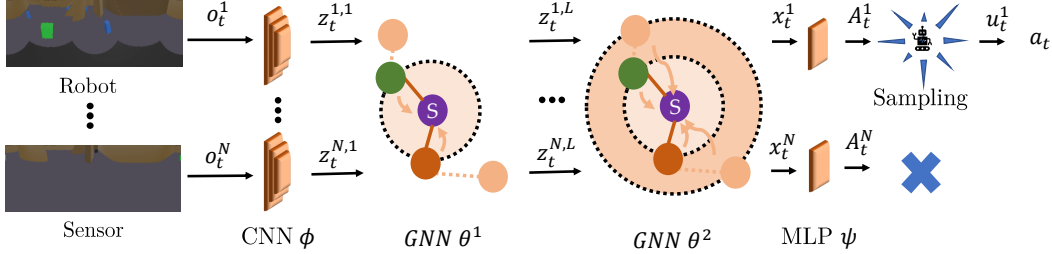


Figure 2: We train a policy in simulation using simulated images o_t^i . The CNN $\phi(\cdot)$ encodes images into features z_t^i and the GNN $\theta(\cdot)$ further encodes this for multiple communication hops in L layers as $z_t^{i,l}$. Eventually, the post-processing MLP $\psi(\cdot)$ generates cost-to-go advantages A_t^i which are used to sample a direction to the target along the shortest path as u_t^i and eventually to generate action a_t for the robot, which is equipped with sensor S_1 .

Neighborhood feature aggregation. In order to predict the target direction, our models need to be able to aggregate information across the whole sensor network. In other words, each sensor requires effective information from those sensors that can *directly* see the target. This feature aggregation task is more challenging than the traditional GNN-based feature aggregation for information prediction [13] or robot coordination tasks [15, 17]. Specifically, in the aforementioned papers, each agent only needs to aggregate information from the nearest few neighbors as their tasks can be achieved by only considering local information. For each agent, information contributed by a very remote agent towards improving the prediction performance can vanish as the network becomes larger. Additionally, in our task, only a limited number of sensors can directly ‘see’ the target. *Yet, crucially, information about the target from these sensors should be transmitted to the whole network, thus enabling all the sensors to predict the target direction from their own location (which is potentially in NLOS)*. In addition, as we do not introduce any global nor relative pose information, in order to predict the target direction, each sensor must implicitly learn the ability to estimate the relative pose to its neighbors by aggregating image features. Furthermore, generating an obstacle-free path in the target direction by only using image features (without knowing the map) is also very challenging.

The multi-layer GNN model $\theta^{(L)}(\cdot)$ consists of L layers and generates a new encoding $z_t^{i,l}$ for each layer L . It takes the image encoding generated by the encoder $z_t^{i,1} = z_t^i$ as input to the first layer, aggregates communicated neighbors’ features using the neighborhood \mathcal{N}^i over multiple layers, and extracts fused features $x_t^i = z_t^{i,L}$ where $z_t^{i,L}$ is the encoding generated by the last GNN layer for each sensor S^i so that $\theta^{(L)}(z_t^i) = x_t^i$.

A GNN model consists of a stack of neural network layers, where each layer aggregates local neighborhood information, i.e., features of neighbors, around each node and then passes this aggregated information on to the next layer. Specifically, our method builds on the GNN layer introduced in [32]. We use a recursive definition for a multi-layer GNN where each layer $L > 0$ computes new features as

$$\theta^{(L)}(z_t^{i,L}) = \sigma\left(\theta^{(L-1)}(z_t^{i,L}) \cdot W_1^{(L)} + \sum_{j \in \mathcal{N}^i} \theta^{(L-1)}(z_t^{j,L}) \cdot W_2^{(L)}\right) \quad (4)$$

that are communicated in the neighborhood \mathcal{N}^i where $W_1^{(L)}$ and $W_2^{(L)}$ are trainable parameter matrices, and σ denotes a component-wise non-linear function, e.g., a sigmoid or a ReLU.

Cost-to-goal prediction. Lastly, we utilize a post-processing Multi-Layer Perceptron (MLP) to predict a set of cost-to-go advantages for each sensor so that $\psi(x_t^i) = A_t^i$, which is eventually used to sample a target direction u_t^i and eventually transform it to an action a_t .

Policy. This results in the composition $\psi \circ \theta \circ \phi(o_t^i) = A_t^i$ to compute a cost-to-go advantages from the local image o_t^i and features $z_t^{i,l}$ communicated through the neighborhood \mathcal{N}^i . We model the set of target directions \mathcal{U} as a discrete distribution so that $u_t^i = \text{cat}(\text{softmax}(-\alpha A_t^i))$ where $\text{cat}(\cdot)$ samples from a categorical distribution and α is a hyperparameter to adjust the stochasticity. As explained in Sec. 3, the relationship between direction u and action a is bijective. Hence, any sensor can be used as part of a mobile robot (to command its motion). In this work, we denote that sensor as S_1 . So far, we have used a

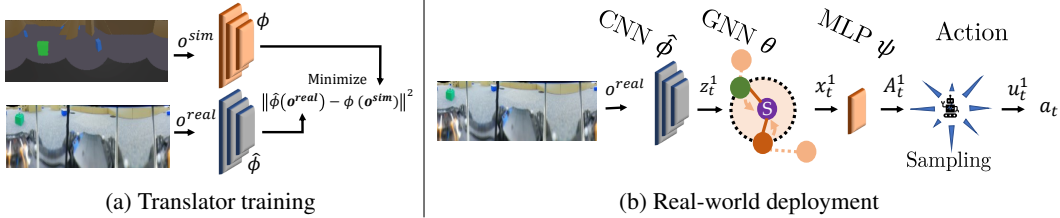


Figure 3: Our sim-to-real framework. (a) After training the policy in simulation, we collect image pairs from simulation o^{sim} and the real world o^{real} and use them to train a real-to-sim translator model $\hat{\phi}$ (gray) by reconstructing latent features from the simulation domain z generated through the encoder trained in simulation ϕ (orange) with real-world images. (b) We combine the translator model $\hat{\phi}$ trained on real-world images (gray) with θ and ψ trained in simulation (orange) to deploy the policy to a real-world setup.

distributed notation to compute a direction u_t^i for any given sensor. We formulate the target navigation problem as centralized MDP relying on a central state $s_t = \{o_t^1, \dots, o_t^N\}$ consisting of the observation of all sensors. Therefore, we can define the policy π as

$$\pi(\{o_t^1, \dots, o_t^N\}) = \text{cat}(\text{softmax}(-\alpha(\psi \circ \theta \circ \phi(o_t^1))))\beta = u_t^1\beta = a_t, \quad (5)$$

where β is a hyperparameter to scale the magnitude and thus transforming a direction into a velocity action $a_t \in \mathcal{A}$. Note that even though the notation of the policy is centralized, the execution is inherently decentralized, and instead of depending on raw image observations for other sensor nodes, the robot only depends on the local observation o_t^1 and latent encodings communicated through the GNN θ . We provide more details on the neural network architecture in [Appendix A](#).

5 Zero-Shot Real World Transfer

To demonstrate the feasibility of a zero-shot transfer of our model, we design a twin environment setup, consisting of both real and digital copies of the operational space, see [Fig. 1](#). The real setup includes custom-built sensors that provide local visual sensing to nearby nodes within the communication network. Later, in [Sec. 6](#), we report results that demonstrate the effectiveness our sim-to-real approach for the real-world scenario. We provide more details on the real-world transfer in [Appendix B](#).

5.1 Setup

Twin Environments. The real-world environment is $5.7 \text{ m} \times 4.2 \text{ m}$, and is cluttered with three to five obstacles of different size. We use standard cardboard boxes for obstacles and blue and green building blocks to identify sensor locations and target location, respectively. In order to facilitate zero-shot transfer, we design a digital twin of our real-world environment. This digital twin (i.e., a simulation environment) is built within the Webots simulator [33] and is illustrated in [Fig. 1](#).

Custom-made sensor nodes. We design and construct six sensor nodes that consist of a contraption holding the downward-facing camera with fisheye lens as well as a local data processing unit. The sensor nodes are equipped with a Raspberry Pi running local processing and image reprojection according to a custom camera calibration procedure, and streaming of image data at a frame rate of 12 Hz. The sensor was designed so that it can be used stand-alone, as well as mounted on a mobile robot.

Mobile robot. We use the DJI RoboMaster as mobile robot platform. A seventh sensor node that also serves as controller for the robot is mounted on top. During navigation, the robot employs a collision shielding mechanism, that takes as input distance measurements to detect the near-sided static obstacles and the border of environment. Repulsive force against detected obstacles are generated through a potential field [34]. This mechanism only triggers for near collisions and is a safety mechanism.

5.2 Domain Adaptation

As outlined in [Fig. 2](#), we first train the policy using simulated images through IL. [Fig. 3](#) outlines how we perform the sim-to-real transfer. We create a real-world environment and map it using a motion capture system. We transfer this map into Webots to have an identical representation of the environment in the real world and in simulation. To train the translator, we tele-operate the robot in this environment to

collect M image pairs of real-world images o_{real} and corresponding simulated images o_{sim} and store them in a dataset $\mathcal{D}_{\text{transfer}} = \{(o_{\text{real}}^j, o_{\text{sim}}^j)\}_{m=0}^M$.

In total, we construct 8 different environments, each populated with 6 sensors and one robot. We collect 2000 image pairs for each sensor in each environment (this is achieved within 5 minutes with images being recorded at 10 Hz). Constructing and mapping each environment and setting up the data collection procedure takes 30 minutes per environment. We automatically filter the images in post processing for the sensor images to only be included when the robot is moving within the field of view of the sensors. This results in a dataset of $M = 80,000$ image pairs for the training set and 10,000 images for the test set.

We use a similar approach to [26], where a neural network based translator model is trained to map real-world images to simulated images, which are then fed to the policy, but instead of mapping to simulated images, we map to their respective encoding. Specifically, we train a translator model $\hat{\phi}(\cdot)$ that maps real images o^{real} to the encoding of the corresponding simulated image $\phi(o^{\text{sim}})$ by minimizing the objective $J_{\text{transfer}}(\cdot)$ while keeping $\phi(\cdot)$ fixed,

$$J_{\text{transfer}}(\hat{\phi}) = \mathbb{E}_{o^{\text{sim}}, o^{\text{real}} \sim \mathcal{D}_{\text{transfer}}} \left[\|\hat{\phi}(o^{\text{real}}) - \phi(o^{\text{sim}})\|^2 \right]. \quad (6)$$

6 Results

We first introduce the metrics we use for evaluation and then demonstrate the performance of our method in simulation, based on the methodology introduced in Sec. 4. Second, we demonstrate successful zero-shot transfer to the real-world setup introduced in Sec. 5. We provide additional results in Appendix C.

6.1 Performance Metrics

We evaluate the trained policies on the unseen test split of the training dataset as well as a generalization set that has been generated with a larger environment and more sensors.

We consider two primary metrics for our evaluation. A run is considered successful if the robot arrives at the target without collisions and within a pre-defined time horizon T , captured by the boolean success indicator C_m for case m . The boolean *success rate* fraction of all successful runs is $\frac{1}{M} \sum_{m=1}^M C_m$. We furthermore report the success weighted by path length, or SPL [35], as $\frac{1}{M} \sum_{m=1}^M C_m \frac{P_m}{\max(p_m, P_m)}$, where P_m is the shortest path length from the robot’s initial position to the target, and p_m the length of the path actually taken. We visualize a selection of paths in Fig. 5. We report all results for environment configurations where the target is within line-of-sight (LOS) initially (therefore trivially solvable without communication) and where the target is in non-line-of-sight (NLOS, therefore requiring additional sensor coverage for an efficient solution) separately.

6.2 Simulations

We train five variants of our policy to evaluate our approach. We first train a policy with communication range $D_S = 0.0$ as a baseline (i.e., no communication). We also train three policies with communication ranges of $D_S = 2.0$, $D_S = 4.0$ and $D_S = \infty$ (fully connected) respectively, all with a single GNN layer. Lastly, we train a policy with a communication range of $D_S = 2.0$ and two GNN layers. The results can be seen in Tab. 1.

We evaluate all policies on $M = 250$ unseen maps on the small test set and $M = 100$ maps on the large test set. All policies have a nearly perfect success rate of close to 1.0 for LOS, which is to be expected as navigating to the target using local information is trivial. The baseline policy without communication has an NLOS success rate of 0.827 and an SPL of 0.719 in the small environment. These values are the lower bound for what is possible without communication. We ensure that all environments are solvable. Even without communication, the target can be discovered through random exploration. The success metrics increase over all experiments with increasing communication ranges, up to 1.0 success and 0.925 SPL for the policy trained with $D_S = 2$ and $L = 1$. The policies with $D_S = 2.0$ and $L = 2$ layers perform similar to the policy with $D_S = 4$. The policy with $D_S = \infty$ and $L = 1$ layers performs slightly worse. This can be attributed to the unfiltered inclusion of information from all sensors. Adding locality through a neighborhood and considering multiple neighborhood through multi-hop communication helps in building a more appropriate global representation.

Table 1: Evaluation of simulation result for five different policies trained for different communication ranges D_S and number of GNN layers L . We report the success rate and SPL for runs where the target was within line-of-sight (LOS) and outside line-of-sight at the start of the experiment (NLOS) as well as the number of samples M on a small test set as well as a generalization set of a larger environment.

D_S	L	Training Distribution ($W = 8, H = 10, N = 7$)				Generalization ($W = 16, H = 20, N = 13$)			
		LOS ($M = 198$)		NLOS ($M = 52$)		LOS ($M = 58$)		NLOS ($M = 42$)	
		Success	SPL	Success	SPL	Success	SPL	Success	SPL
0.0	1	1.000	0.958	0.827	0.719	1.000	0.945	0.619	0.492
2.0	1	1.000	0.963	1.000	0.925	0.983	0.935	0.833	0.742
4.0	1	1.000	0.963	0.981	0.912	1.000	0.945	0.905	0.804
2.0	2	1.000	0.964	1.000	0.909	1.000	0.954	0.857	0.756
∞	1	1.000	0.962	0.962	0.880	1.000	0.940	0.952	0.853

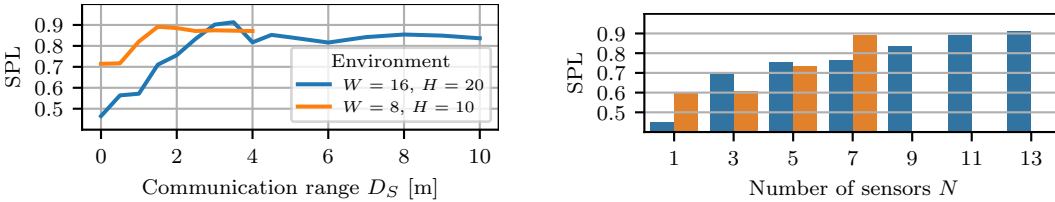


Figure 4: We record the performance of the policy trained for $D_S = 2$ and $L = 2$ for a range of different communication ranges and number of sensors. Left: The large environment (blue) is populated with $N = 13$ sensors and the small environment (orange) with $N = 7$ sensors. Right: The large environment (blue) has a communication range of $D_S = 3.5m$ and the small environment (orange) of $D_S = 1.5m$. Both values result in peak performance for the maximum number of sensors in the corresponding environment, as can be seen on the left side. It can be seen that increasing communication range and number of sensors benefits the SPL.

We furthermore test the generalizability to larger environments. The baseline policy has a success rate of 0.619 and an SPL of 0.492, while the fully connected policy has a success rate of up to 0.952 and an SPL of 0.853.

In Fig. 4 we further analyze the benefit of communication on our method. We use the policy trained for $D_S = 2$ and $L = 2$ on the small and the large test set and evaluate the performance for a variety of communication ranges and number of sensors. Note that the results in Tab. 1 for the large environment are suboptimal due to the constrained communication range, since $D_S = 2.0$ for $L = 2$ covers sensors at most 4.0 m away, while the maximum environment length is 14.0 m. We find that the SPL in the large environment increases approximately linearly from 0.45 for $D_S = 0.0$ to 0.91 for $D_S = 3.5$ and then slightly decreases to a constant of 0.85 for $D_S \geq 4.0$, resulting in a performance increase of $2.0\times$ compared to the communication-free baseline. The small environment performs at 0.72 SPL without communication and 0.93 with communication, resulting in a $1.3\times$ performance increase. Decreasing the number of sensors correspondingly decreases the SPL for a similar minimum and maximum performance. It is to be expected that both environments perform similarly well with the maximum number of sensors and a communication range that results in a coverage of the whole environment, whereas in the no communication case and with only one sensor, the small environment performs better (since less exploration is required to navigate to the target).

6.3 Sim-to-Real Policy Transfer

After performing the domain adaptation, we evaluate the performance of the policy on the real-world setup as described in Sec. 5. We use a motion capture system to create a map of the environment and track the robot and target position for the evaluation. We construct three different environments, two of which are taken from the test set (Env. A and B) and a random environment (Env. C) created by us with a similar sensor layout to Env. B but with a different obstacle placement. We run 25 evaluation runs for each environment, resulting in a total of 75 evaluation runs, of which 66 are NLOS runs.

The results for all environments are shown in Fig. 5. The total success rate across all environments is 0.745 and 0.577 SPL for NLOS. Environment A is the least challenging environment, with only three

Env	LOS		NLOS	
	Success	SPL	Success	SPL
A	0.833	0.679	0.895	0.662
B	0.875	0.791	0.625	0.497
C	1.000	0.897	0.700	0.559
All	0.895	0.783	0.745	0.577

(a) Real-world results

(b) Env. A

(c) Env. B

(d) Env. C

Figure 5: (a) Evaluation of real-world results for three different environments for the fully connected policy. We report success rate and SPL for runs where the target was within line-of-sight (LOS, $M_A = 2$, $M_B = 5$, $M_C = 1$) and outside line-of-sight at the start of the experiment (NLOS, $M_A = 23$, $M_B = 19$, $M_C = 24$). (b, c, d) A selection of two policy evaluations for NLOS configurations for each real-world environment. Blue squares indicate sensor positions, the green square the target position q^G , the red path the robot’s initial position q_0^R , the red path the shortest path computed by the expert P and the orange path the path p chosen by the policy π .

small obstacles in total, and has the highest NLOS success rate of 0.895 and SPL of 0.662. Environment B is, with an NLOS success rate of 0.625, the most challenging one, with a total of five obstacles, ranging from small to large, and narrow passages between obstacles. Environment C is a variation of Environment B and lies in between Environment A and C with an NLOS success rate of 0.7 and an SPL of 0.577. Even though the sim-to-real transfer is generally successful, there is a noticeable reality gap. We found that the real-world sensors have a much smaller visibility range than the simulated sensors, and even though we did not conduct any real-world baseline experiments, it is to be expected that the SPL for $D_S = 0$ (i.e., no communication) would be significantly smaller.

7 Limitations

All communication between sensors is synchronous, and we do not consider any communication time delays or message dropouts. Asynchronous evaluation and message delays can negatively affect the performance of GNN-based control policies [28]. These effects could potentially be counteracted by incorporating such message delays into the training procedure.

The target must be within line-of-sight of *at least one* sensor within multi-hop communication to the sensor node attached to the mobile robot. In future work, this problem can be resolved by replacing the static sensors with mobile robots that dynamically cover the environment.

Due to limitations of the expert solver, our current approach does not consider dynamic obstacles. This limitation can be alleviated by using a more capable solver or augmenting our learning paradigm to include interactive components (e.g., through Reinforcement Learning).

Lastly, the local coordinates of the robot and all the sensors are aligned, i.e. they are facing the same direction. We do not assume knowledge of the global nor relative positioning of the robot or sensors. This limitation can be circumvented by using a magnetic field sensor to align the visual sensors or by introducing a random rotation of cameras into the dataset to learn an equivariant mapping of the camera heading. Due to architectural constraints, learning this can be challenging, and rotation equivariant architectures such as [36] have to be considered.

8 Conclusions

In this paper, we propose a vision-only-based learning approach that leverages a Graph Neural Network (GNN) to encode and communicate relevant viewpoint information to the mobile robot. In our experiments, we first demonstrate generalization to previously unseen environments with various sensor layouts. Our results show that by using communication between the sensors and the robot, we achieve a $1.3\times$ improvement on small environments and a $2.0\times$ improvement in SPL on large environments, when compared to the communication-free baseline, hence showing increasing improvement for larger environment sizes. This is done without requiring a global map, positioning data, nor pre-calibration of the sensor network. The benefit of utilizing communication in wireless sensor networks increases as the size of the environment increases, since the robot is less likely to discover the goal through random (unguided) exploration using the communication-free baseline. We perform a zero-shot transfer of our model from simulation to the real world. To this end, we train a translator model that translates between

real and simulated images so that the navigation policy (which is trained entirely in simulation) can be used directly on the real robot, without additional fine-tuning. Physical experiments demonstrate first-of-a-kind results that show successful real-world demonstrations on a practical robotic platform with raw visual inputs.

Acknowledgement

This work was supported by European Research Council (ERC) Project 949949 (gAIA). J. Blumenkamp acknowledges the support of the 'Studienstiftung des deutschen Volkes' and an EPSRC tuition fee grant. This research is funded in part by a gift from Arm. Their support is gratefully acknowledged.

References

- [1] P. W. Mirowski, R. Pascanu, F. Viola, H. Soyer, A. Ballard, A. Banino, M. Denil, R. Goroshin, L. Sifre, K. Kavukcuoglu, D. Kumaran, and R. Hadsell. Learning to navigate in complex environments. *ArXiv*, abs/1611.03673, 2017.
- [2] A. Kolling and S. Carpin. Surveillance strategies for target detection with sweep lines. In *IEEE/RSJ International Conference on Intelligent Robots and Systems*, pages 5821–5827, 2009.
- [3] P. Corke, R. Peterson, and D. Rus. Networked robots: Flying robot navigation using a sensor net. In *International Symposium on Robotics Research*, pages 234–243, 2005.
- [4] Z. Kashino, G. Nejat, and B. Benhabib. A hybrid strategy for target search using static and mobile sensors. *IEEE Transactions on Cybernetics*, 50(2):856–868, 2020.
- [5] S. Shenoy and J. Tan. Simultaneous localization and mobile robot navigation in a hybrid sensor network. In *IEEE/RSJ International Conference on Intelligent Robots and Systems*, pages 1636–1641, 2005.
- [6] M. A. Batalin, G. S. Sukhatme, and M. Hattig. Mobile robot navigation using a sensor network. volume 1, pages 636–641, 2004.
- [7] Q. Li, M. DeRosa, and D. Rus. Distributed algorithms for guiding navigation across a sensor network. In *International Conference on Mobile Computing and Networking*, pages 313–325, 2003.
- [8] D. Shah and L. Vachhani. Swarm aggregation without communication and global positioning. *IEEE Robotics and Automation Letters*, 4(2):886–893, 2019.
- [9] J. Ortiz, T. Evans, and A. J. Davison. A visual introduction to gaussian belief propagation. *arXiv preprint arXiv:2107.02308*, 2021.
- [10] F. Dellaert, R. Roberts, V. Agrawal, A. Cunningham, C. Beall, D.-N. Ta, F. Jiang, lucacarlone, nikai, J. L. Blanco-Claraco, S. Williams, ydjian, J. Lambert, A. Melim, Z. Lv, A. Krishnan, J. Dong, G. Chen, K. Chande, balderdash devil, DiffDecisionTrees, S. An, mpaluri, E. P. Mendes, M. Bosse, A. Patel, A. Baid, P. Furgale, matthewbroadwaynavenio, and roderick koehle. borglab/gtsam, May 2022. URL <https://doi.org/10.5281/zenodo.5794541>.
- [11] G. M. Bhatti. Machine learning based localization in large-scale wireless sensor networks. *Sensors*, 18(12):4179, 2018.
- [12] M. Jaderberg, V. Mnih, W. M. Czarnecki, T. Schaul, J. Z. Leibo, D. Silver, and K. Kavukcuoglu. Reinforcement learning with unsupervised auxiliary tasks. *ArXiv*, abs/1611.05397, 2017.
- [13] S. S. Akter and L. B. Holder. Improving iot predictions through the identification of graphical features. *Sensors*, 19(15):3250, 2019.
- [14] Q. Li, F. Gama, A. Ribeiro, and A. Prorok. Graph neural networks for decentralized multi-robot path planning. pages 11785–11792, 2020.
- [15] Q. Li, W. Lin, Z. Liu, and A. Prorok. Message-aware graph attention networks for large-scale multi-robot path planning. *IEEE Robotics and Automation Letters*, 6:5533–5540, 2021.
- [16] J. Blumenkamp and A. Prorok. The emergence of adversarial communication in multi-agent reinforcement learning. 2020.
- [17] T.-K. Hu, F. Gama, T. Chen, Z. Wang, A. Ribeiro, and B. M. Sadler. Vgai: End-to-end learning of vision-based decentralized controllers for robot swarms. In *ICASSP 2021-2021 IEEE International Conference on Acoustics, Speech and Signal Processing (ICASSP)*, pages 4900–4904. IEEE, 2021.
- [18] S. Ross and D. Bagnell. Efficient reductions for imitation learning. In Y. W. Teh and M. Titterton, editors, *International Conference on Artificial Intelligence and Statistics*, volume 9 of *Proceedings of Machine Learning Research*, pages 661–668, Chia Laguna Resort, Sardinia, Italy, 13–15 May 2010. PMLR. URL <https://proceedings.mlr.press/v9/ross10a.html>.

- [19] S. Ross, G. J. Gordon, and J. A. Bagnell. A reduction of imitation learning and structured prediction to no-regret online learning, 2011. URL <https://arxiv.org/abs/1011.0686>.
- [20] S. Ross and J. A. Bagnell. Reinforcement and imitation learning via interactive no-regret learning, 2014. URL <https://arxiv.org/abs/1406.5979>.
- [21] M. Bhardwaj, S. Choudhury, and S. Scherer. Learning heuristic search via imitation. In *Conference on Robot Learning*, pages 271–280, 2017.
- [22] T. Zhang, G. Kahn, S. Levine, and P. Abbeel. Learning deep control policies for autonomous aerial vehicles with mpc-guided policy search. In *2016 IEEE International Conference on Robotics and Automation (ICRA)*, pages 528–535, 2016. doi:10.1109/ICRA.2016.7487175.
- [23] S. James, P. Wohlhart, M. Kalakrishnan, D. Kalashnikov, A. Irpan, J. Ibarz, S. Levine, R. Hadsell, and K. Bousmalis. Sim-to-real via sim-to-sim: Data-efficient robotic grasping via randomized-to-canonical adaptation networks. In *IEEE/CVF Conference on Computer Vision and Pattern Recognition*, pages 12627–12637, 2019.
- [24] A. Church, J. Lloyd, R. Hadsell, and N. F. Lepora. Tactile sim-to-real policy transfer via real-to-sim image translation. In *Conference on Robot Learning*, pages 1645–1654. PMLR, 2022.
- [25] P. Isola, J.-Y. Zhu, T. Zhou, and A. A. Efros. Image-to-image translation with conditional adversarial networks. In *IEEE Conference on Computer Vision and Pattern Recognition (CVPR)*, pages 5967–5976, 2017.
- [26] J. Zhang, L. Tai, P. Yun, Y. Xiong, M. Liu, J. Boedecker, and W. Burgard. Vr-goggles for robots: Real-to-sim domain adaptation for visual control. *IEEE Robotics and Automation Letters*, 4(2): 1148–1155, 2019.
- [27] J.-Y. Zhu, T. Park, P. Isola, and A. A. Efros. Unpaired image-to-image translation using cycle-consistent adversarial networks. In *IEEE International Conference on Computer Vision (ICCV)*, pages 2242–2251, 2017.
- [28] J. Blumenkamp, S. D. Morad, J. Gielis, Q. Li, and A. Prorok. A framework for real-world multi-robot systems running decentralized gnn-based policies. In *IEEE International Conference on Robotics and Automation*, 2022.
- [29] M. Bhardwaj, S. Choudhury, and S. Scherer. Learning heuristic search via imitation. In *Conference on Robot Learning*, pages 271–280. PMLR, 2017.
- [30] S. Ross and J. A. Bagnell. Reinforcement and imitation learning via interactive no-regret learning. *ArXiv*, abs/1406.5979, 2014.
- [31] M. Sandler, A. G. Howard, M. Zhu, A. Zhmoginov, and L.-C. Chen. Mobilenetv2: Inverted residuals and linear bottlenecks. In *IEEE Conference on Computer Vision and Pattern Recognition*, June 2018.
- [32] C. Morris, M. Ritzert, M. Fey, W. L. Hamilton, J. E. Lenssen, G. Rattan, and M. Grohe. Weisfeiler and leman go neural: Higher-order graph neural networks. In *AAAI*, volume 33, pages 4602–4609. AAAI Press, 2019.
- [33] O. Michel. Webots: Professional mobile robot simulation. *Journal of Advanced Robotics Systems*, 1(1):39–42, 2004. URL <http://www.ars-journal.com/International-Journal-of-Advanced-Robotic-Systems/Volume-1/39-42.pdf>.
- [34] Y. K. Hwang and N. Ahuja. A potential field approach to path planning. *IEEE Transactions on Robotics and Automation*, 8(1):23–32, 1992.
- [35] P. Anderson, A. Chang, D. S. Chaplot, A. Dosovitskiy, S. Gupta, V. Koltun, J. Kosecka, J. Malik, R. Mottaghi, M. Savva, et al. On evaluation of embodied navigation agents. *arXiv preprint arXiv:1807.06757*, 2018.

- [36] N. Thomas, T. Smidt, S. Kearnes, L. Yang, L. Li, K. Kohlhoff, and P. Riley. Tensor field networks: Rotation-and translation-equivariant neural networks for 3d point clouds. *arXiv preprint arXiv:1802.08219*, 2018.
- [37] D. Coleman. Lee's $O(n^2 \log n)$ visibility graph algorithm implementation and analysis, 2012.
- [38] Z. Zhang. A flexible new technique for camera calibration. *IEEE Transactions on pattern analysis and machine intelligence*, 22(11):1330–1334, 2000.
- [39] B. Li, L. Heng, K. Koser, and M. Pollefeys. A multiple-camera system calibration toolbox using a feature descriptor-based calibration pattern. In *IEEE/RSJ International Conference on Intelligent Robots and Systems*, pages 1301–1307. IEEE, 2014.
- [40] C. Mei and P. Rives. Single view point omnidirectional camera calibration from planar grids. In *IEEE International Conference on Robotics and Automation*, pages 3945–3950. IEEE, 2007.
- [41] A. Shankar, S. G. Elbaum, and C. Detweiler. Freyja: A full multirotor system for agile & precise outdoor flights. In *IEEE International Conference on Robotics and Automation*, pages 217–223. IEEE, 2021.

Appendices

A Parameters

A.1 Dataset

In order to train the policy π , we imitate an expert path planner that operates in the continuous domain. The dataset is composed of random environment layouts and sensor placements. Each environment in the dataset has the same dimension $W \times H$ but is populated with a random number of obstacles of variable size. Obstacles are placed with a constraint on distance to other obstacles so that each obstacle C is placed not closer than D_{\min}^C to any other obstacle. After placing obstacles, the target and sensors S^2, \dots, S^N are placed randomly in the environment, with the same distance constraint between sensors and obstacles, but with a separate distance constraint D_{\min}^S between sensors and sensors. Lastly, the sensor node S^1 representing the robot R is placed with a distance of at least D_{\min}^R to any obstacle or sensor. Eventually, we construct a visibility graph on an expanded map that accounts for the size of the robot, and we compute the shortest path from all sensors and the robot to the target using an any-angle variation of Lee’s algorithm [37] computing a path $\mathcal{P}(q_0^R, q^G)$. If no valid path can be found for any of the sensors or robot, the map is discarded.

The dataset for all experiments, unless otherwise specified, contains environments of size $W \times H$ where $W = 9$ and $H = 12$, both units are number of boxes. Each box has a size of $0.5 \text{ m} \times 0.3 \text{ m} \times 0.3 \text{ m}$, which is similar to the boxes used in the real-world setup. When placing obstacles, each obstacle is placed at least $D_{\min}^C = 0.51 \text{ m}$ from any other obstacle, including the border. The robot and sensors are placed at a similar distance between each other and any obstacle, so that $D_{\min}^R = D_{\min}^C$. This is to ensure that the robot can always pass between any two sensors or obstacles. $N = 6$ Sensors are placed with a distance of $D_{\min}^S = 0.75$ between each other, to avoid a placement of multiple sensors too close to each other.

We compute 40000 environment layouts and then render the sensor views in Webots. We assume that sensor cameras are placed facing downwards with a fisheye lens, resulting in a 360° view of the environment. Due to OpenGL constraints, Webots does not support rendering of fisheye lenses. Instead, it supports a mode in which six camera images are automatically stitched together into a projection similar to a fisheye projection. Specifically, it projects the merged image to a square of configurable size, in our case $320 \text{ px} \times 320 \text{ px}$. We post-process this by projecting from a square to a circle and then projecting to a polar representation, using OpenCV, resulting in images of size $320 \text{ px} \times 120 \text{ px}$.

An environment sample, the corresponding environment in Webots and sensor samples can be seen in Fig. 6.

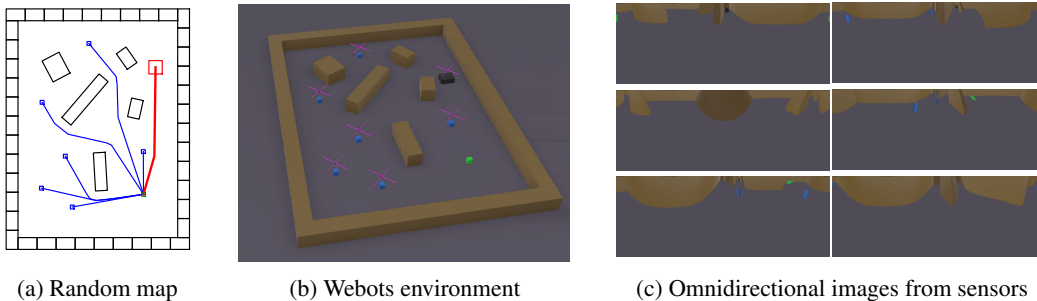


Figure 6: Generation of training data. (a) We first create random maps; in the illustration, blue points are sensor locations, the red square is the robot, green square is the target and corresponding lines indicate the shortest path from sensors and robots to the target. Black boxes indicate obstacles. (b) Random maps are rendered in 3D in the simulation environment, Webots. Sensors are blue, the target is green, the boxes brown and the robot black. (c) Sensors are equipped with omnidirectional cameras.

A.2 Training

Policy. We use supervised learning to predict the pre-computed cost-to-go advantages. We predict $K = 8$ advantages (unless specified otherwise). The minibatch size is 16. The dataset contain 40000 samples, of which we use 80% for training, 29% for evaluation and 1% for testing. The test set is used for all evaluations and path visualization in this paper. The learning rate is 0.001 with an exponential decay of 0.98 with a seed of 1265. All experiments are trained for 200 training iterations, and the experiments with the best performance on the evaluation set is used to avoid overfitting. For evaluation, we use the L1 distance (mean absolute error) between predicted and ground truth cost-to-go advantages. We train with 16-bit floating-point precision.

Domain Adaptation. Training the translator is done with similar settings as the policy. We use the L2 distance (mean squared error) to evaluate the performance on the evaluation test. We use image augmentation to artificially increase the size of the dataset to avoid overfitting and increase robustness. We perform shifting (specifically rolling, as the image is a 360° view of the environment) of both the real image and the corresponding simulated image. We apply a random change of 50% to 150% in brightness, a random shift of $\pm 9^\circ$ in the hue color space, a random change of $\pm 10\%$ in contrast and $\pm 5\%$ in saturation as well as a random affine transformation with a rotation of $\pm 3^\circ$, a translation and scale of $\pm 3\%$ and a shear of $\pm 3^\circ$ to the real image. Samples of this augmentation are also depicted in row 3 of Fig. 8.

A.3 Neural Network Architecture

The CNN is split in two halves for the sim-to-real domain adaptation process, where the first half creates an internal latent embedding as $\phi_{\text{PRE}} = y$ and the second half the communicated output features z so that $\phi(o) = \phi_{\text{POST}}(\phi_{\text{PRE}}(o)) = z$.

The feature extractor $\phi(\cdot)$ uses MobileNet v2 [31] to extract features z from the input omnidirectional image o . ϕ_{PRE} contains the first 14 residuals and ϕ_{POST} all others. The latent encoding z is a vector of size 64. We use PyTorch Geometric’s GraphConv implementation for GNN layers with an output size of 256. The post-processing MLP consists of four layers with 128, 64, 64 and 64 neurons each and an output size of K for the number of cost-to-go advantages.

B Real-world Experiments

The environment in Webots was co-designed with the real-world setup used for our experiments. We use cardboard paper boxes of size $0.5 \text{ m} \times 0.3 \text{ m} \times 0.3 \text{ m}$ as obstacle and colored building boxes of size $0.1 \text{ m} \times 0.1 \text{ m} \times 0.1 \text{ m}$ as sensor and target indicator. As sensor, we use a Raspberry Pi High Quality Camera equipped with a lens with a field of view (FOV) of 180° . The camera is connected to a Raspberry Pi 4 that runs Ubuntu 20.04 and ROS2 Foxy and performs image reading, performs projection from raw image to equirectangular [38] images, compression and streaming at a frame rate of 12 Hz. We use OpenCV and a custom-made camera calibration tool [39, 40] that allows us to automate most of the image calibration and cropping required to run the policy.

We use the same sensor contraption on the mobile robot. The Raspberry Pi is connected to the RoboMaster and performs low-level control using a custom made interface to the RoboMaster and the Freyja control suite [41].

B.1 Real World Dataset Collection

We construct eight different environments and create a map using a motion capture system that we then transfer into our Webots simulation. A sample of a Twin Environment setup can be seen in Fig. 7. We remote-control the robot manually while recording synchronized real and corresponding simulated images.

B.2 Interpreter

To verify the functionality of our translator, which generates latent image encodings from real-world images, and to support debugging in the real-world deployment, we train a decoder $\phi^{-1}(\cdot)$ that maps the

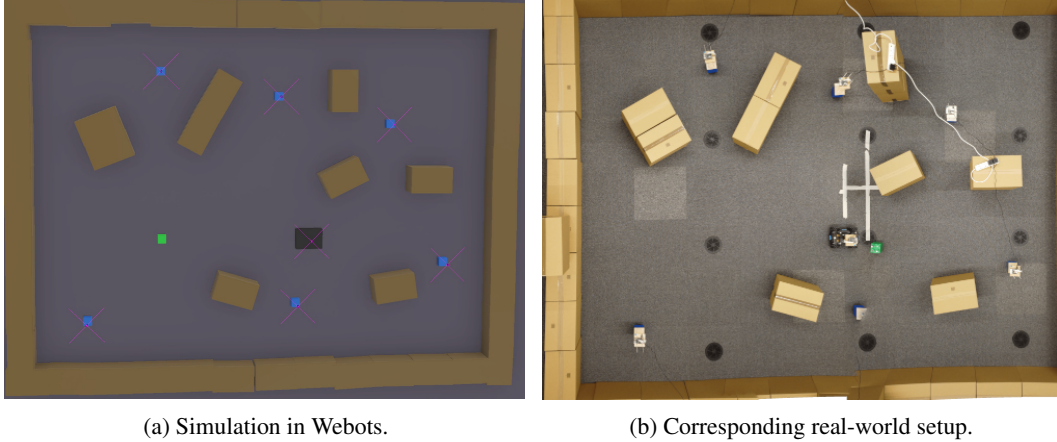


Figure 7: Sample of the Twin Environment setup. The simulated environment in Webots can be seen on the left, and the corresponding real-world environment on the right. Note the matching position and alignment of environment size and obstacles.

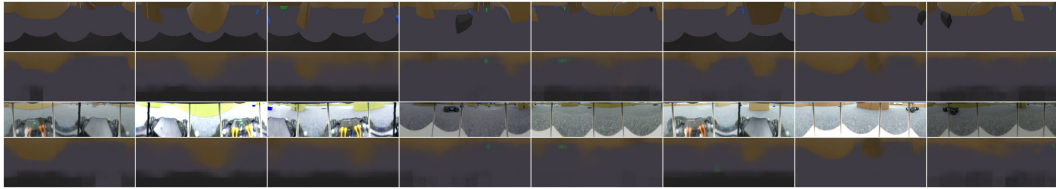


Figure 8: Samples of the interpreter used to convert latent image encodings into interpretable images. Columns: 8 independent samples. First row: Simulated image o^{sim} . Second row: The image in the first row is encoded as $z^{\text{sim}} = \phi(o^{\text{sim}})$ and reconstructed as $\phi^{-1}(z^{\text{sim}})$. Third row: Corresponding real-world image o^{real} . Fourth row: Reconstruction of the simulated image from the real image as $o^{\text{realto sim}} = \phi^{-1}(\phi_{\text{POST}}(\hat{\phi}(o^{\text{real}})))$.

latent encodings z back to image observations o . Samples of reconstructions generated by the translator and the interpreter can be seen in Fig. 8.

C Results

C.1 Trajectories

In the following panels, we show all evaluation runs from the three real-world environments in Fig. 10 (Environment A), Fig. 11 (Environment B), and Fig. 12 (Environment C).

We also report a broader selection of path evaluations in simulation in Fig. 13.

C.2 Number of cost-to-go advantages

We compare the effect a varying number of cost-to-go advantages have on the policy. We compute $K = 8$ and $K = 16$ cost-to-go advantages and train two policies. The results can be seen in Tab. 2 and show that the overall success rate increases and detour decreases with a larger K .

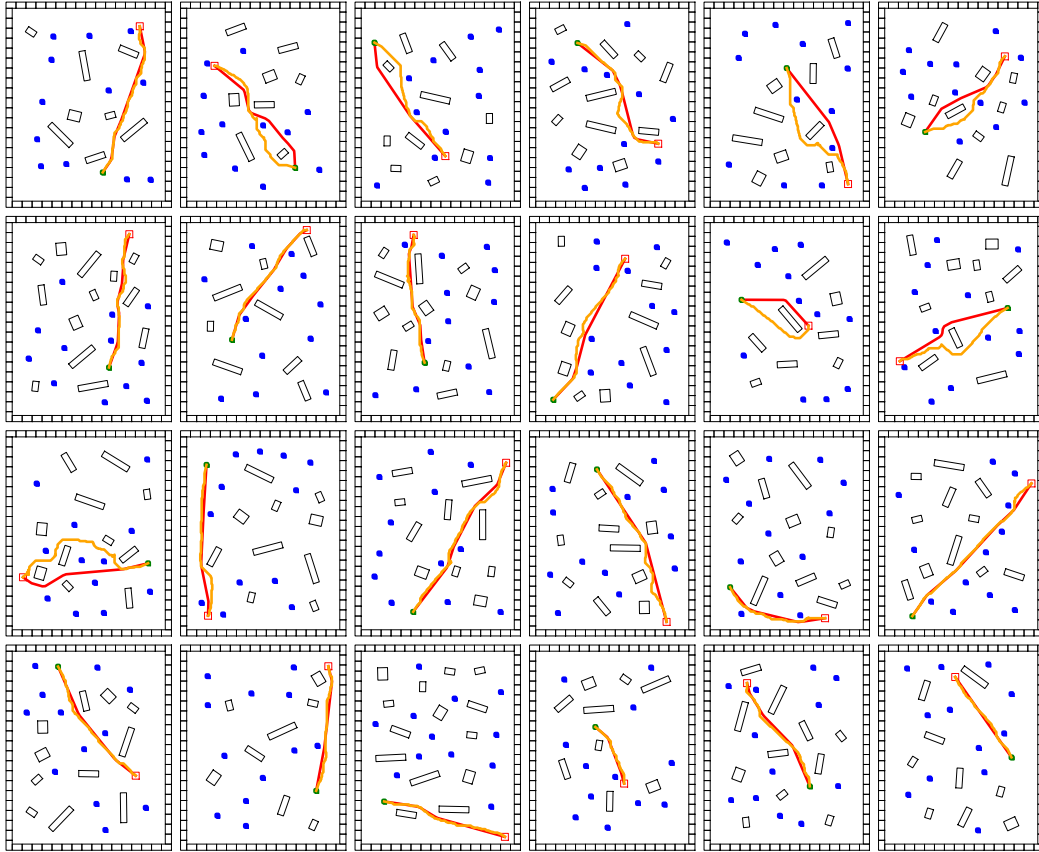


Figure 9: Generalizability to larger environments and larger number of agents $N = 13$ for GNN layers $L = 2$ and communication range $D_S = 3.5$ m (SPL 0.91). Blue squares indicate sensor positions, the green square the target position q^G , the red path the robot's initial position q_0^R , the red path the shortest path computed by the expert and the orange path the path chosen by the policy π .

Table 2: Analysis of the effect of number of cost-to-go advantages on performance.

K	LOS		NLOS	
	Success	SPL	Success	SPL
8	1.000	0.945	0.837	0.711
16	1.000	0.967	0.913	0.801

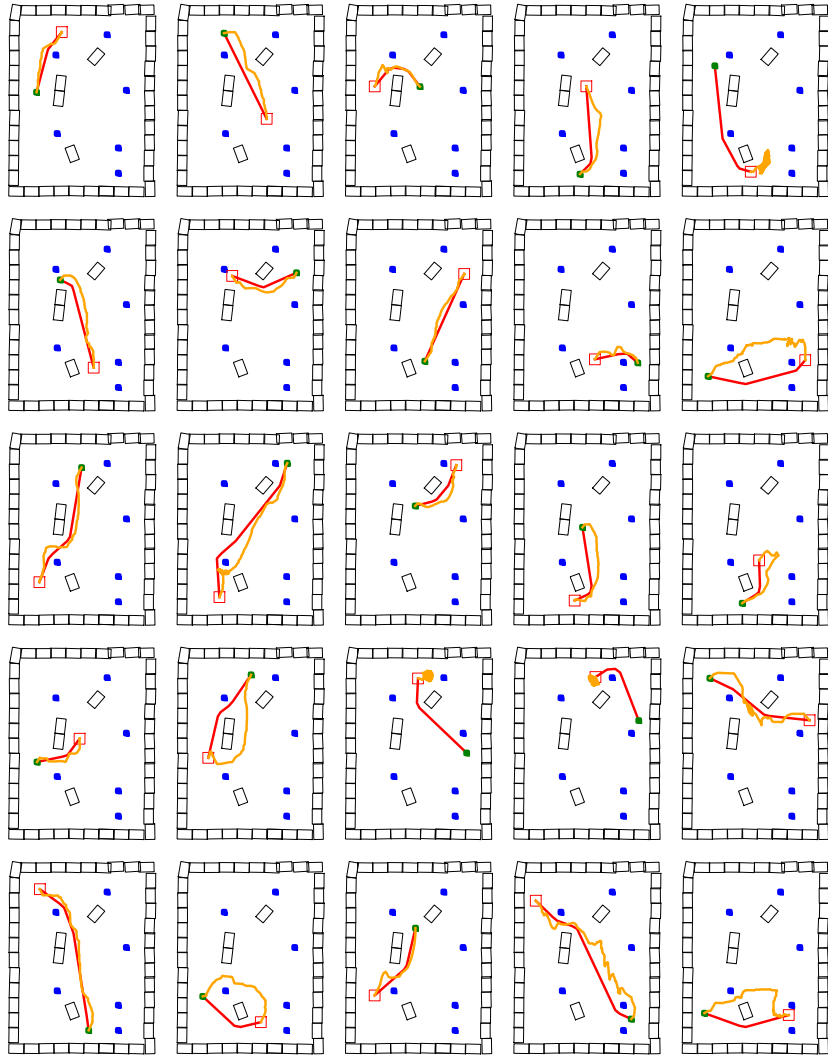


Figure 10: All real-world evaluations for Environment A. Blue squares indicate sensor positions, the green square the target position q^G , the red path the robot's initial position q_0^R , the red path the shortest path computed by the expert and the orange path the path chosen by the policy π .

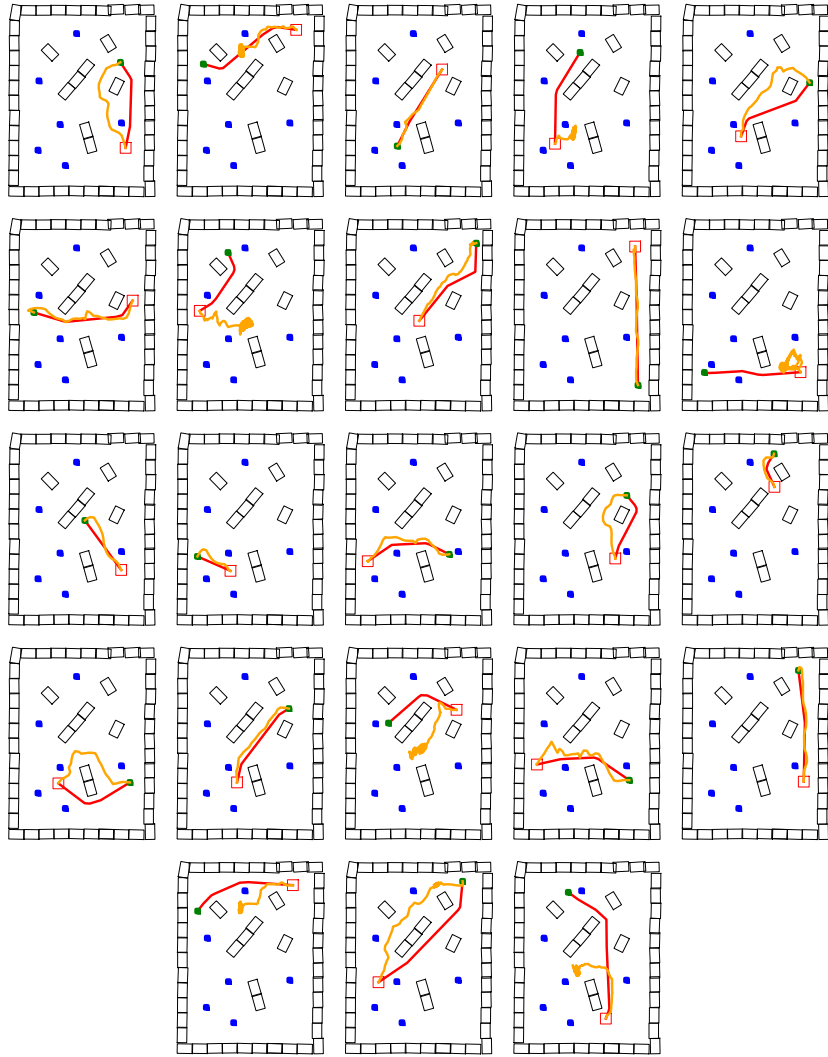


Figure 11: All real-world evaluations for Environment B. Blue squares indicate sensor positions, the green square the target position q^G , the red path the robot's initial position q_0^R , the red path the shortest path computed by the expert and the orange path the path chosen by the policy π .

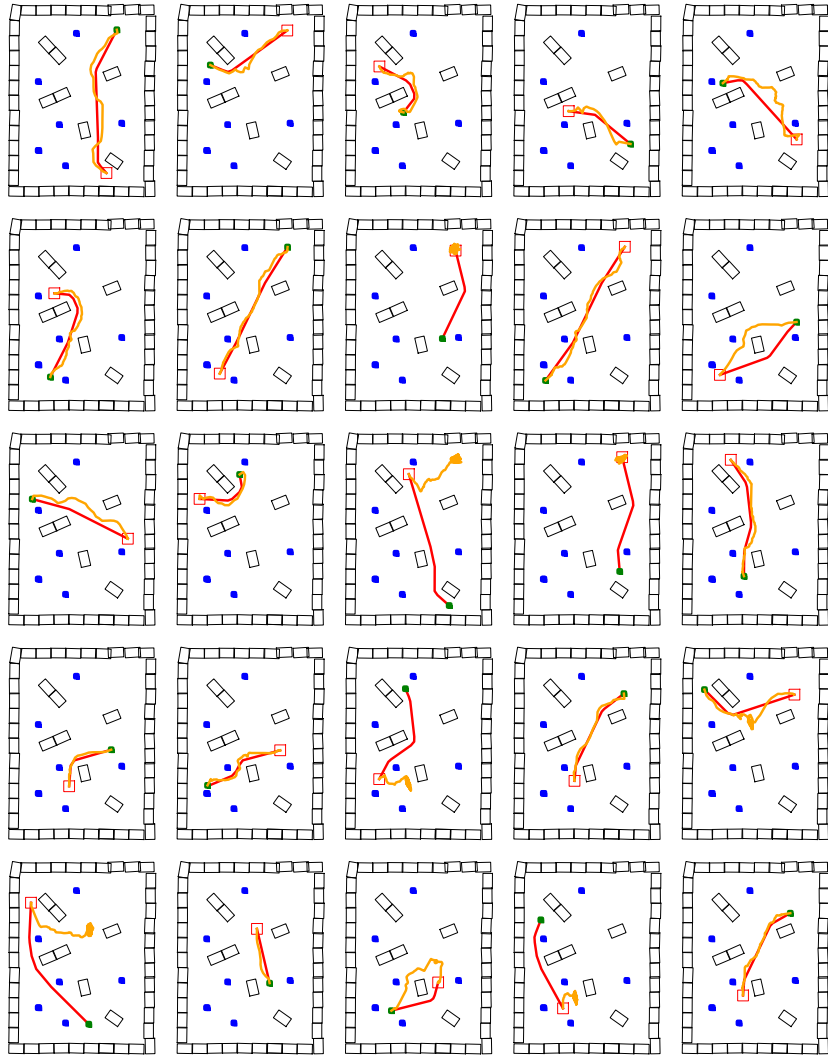


Figure 12: All real-world evaluations for Environment C. Blue squares indicate sensor positions, the green square the target position q^G , the red path the robot's initial position q_0^R , the red path the shortest path computed by the expert and the orange path the path chosen by the policy π .

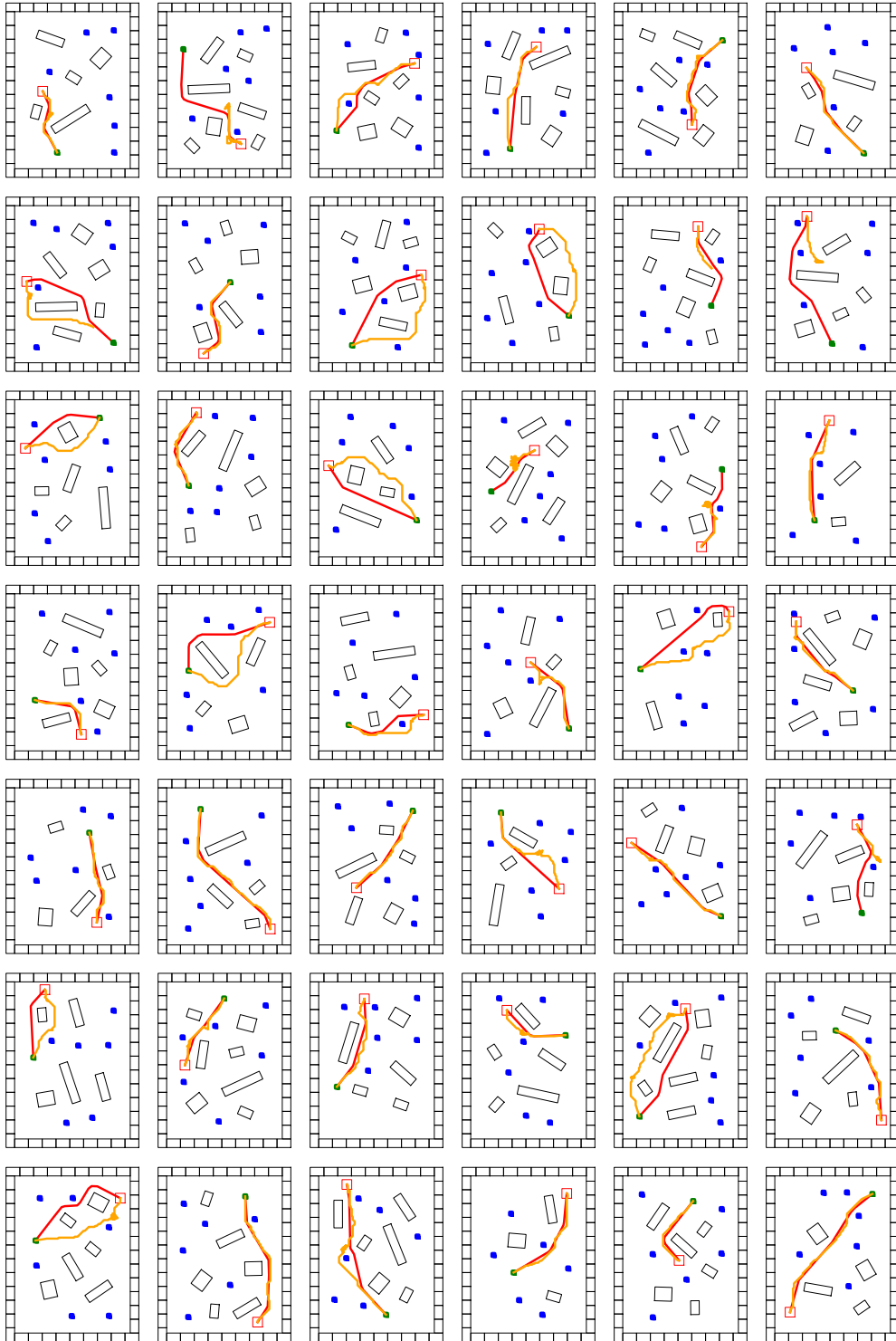


Figure 13: A selection of policy evaluations for NLOS configurations in simulation. Blue squares indicate sensor positions, the green square the target position q^G , the red path the robot's initial position q_0^R , the red path the shortest path computed by the expert and the orange path the path chosen by the policy π .